HHS Public Access

Author manuscript

Biochemistry. Author manuscript; available in PMC 2019 August 02.

Published in final edited form as:

Biochemistry. 2019 April 02; 58(13): 1709–1717. doi:10.1021/acs.biochem.8b01124.

Structural basis of lysosomal phospholipase A_2 inhibition by Zn^{2+}

Renee A. Bouley[†], **Vania Hinkovska-Galcheva**[‡], **James A. Shayman**[‡], **John J. G. Tesmer**[*,§]

[†]Life Sciences Institute and Department of Pharmacology, University of Michigan, Ann Arbor, Michigan 48109, United States

[‡]Department of Internal Medicine, University of Michigan Medical School, University of Michigan, Ann Arbor, Michigan 48109, United States

[§]Departments of Biological Sciences and of Medicinal Chemistry & Molecular Pharmacology, Purdue University, West Lafayette, Indiana 47907, United States

Abstract

Lysosomal phospholipase A_2 (LPLA$_2$/PLA2G15) is a key enzyme involved in lipid homeostasis and is characterized by both phospholipase A2 and transacylase activity, and an acidic pH optimum. Divalent cations such as Ca^{2+} and Mg^{2+} have previously been shown to have little effect on the activity of LPLA$_2$, but the discovery of a novel crystal form of LPLA$_2$ with Zn^{2+} bound in the active site suggested a role for this divalent cation in regulating enzyme activity. In this complex, the cation directly coordinates the serine and histidine of the α/β-hydrolase triad and stabilizes a closed conformation. This closed conformation is characterized by an inward shift of the lid loop, which extends over the active site, which effectively blocks access to one of its lipid acyl chain binding tracks. Therefore, we hypothesized that Zn^{2+} would inhibit LPLA$_2$ activity at a neutral but not acidic pH due to the fact that histidine would be positively charged at lower pH. Indeed, Zn^{2+} was found to inhibit the esterase activity of LPLA$_2$ in a noncompetitive manner exclusively at a neutral pH (between 6.5 and 8.0). Because lysosomes are reservoirs of Zn^{2+} in cells, the pH optimum of LPLA$_2$ might allow it to catalyze acyl transfer unimpeded within the organelle. We conjecture that Zn^{2+} inhibition of LPLA$_2$ at higher pH maintains lower activity of the esterase in environments where its activity is not typically required.

Graphical Abstract:

[*]**Corresponding Author:** jtesmer@purdue.edu, Phone: (765) 494-1807.

Author Contributions

The manuscript was written through contributions of all authors. All authors have given approval to the final version of the manuscript.

ASSOCIATED CONTENT

Accession Codes

The coordinates of the LPLA$_2$·Zn^{2+} structure have been deposited in the Protein Data Bank with the accession code of 6MTW. UniProt Accession ID: Q8NCC3.

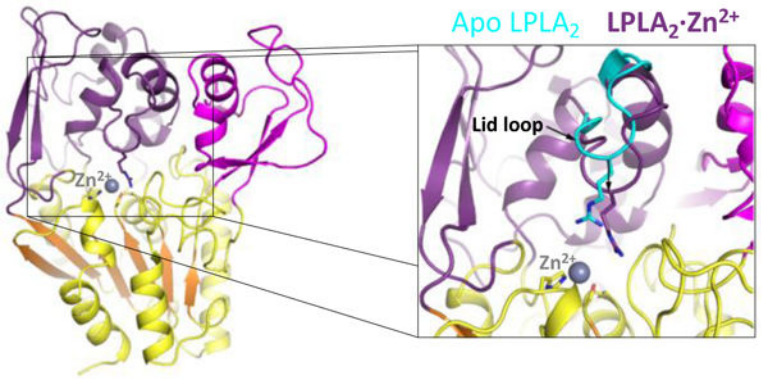

Keywords

Acyltransferase; lysosome; phospholipase A_2 group XV; crystallography; Zn^{2+}

INTRODUCTION

Lysosomal phospholipase A_2 ($LPLA_2$ /PLA2G15) is a ubiquitous enzyme most highly expressed in alveolar macrophage and acts on glycerophospholipids as both a phospholipase and an acyltransferase. $LPLA_2$ has a pH optimum of 4.5, consistent with its localization in the lysosome, and $LPLA_2$ knockout mice develop a phenotype consistent with phospholipidosis.[1] The enzyme belongs to the α/β-hydrolase superfamily and consequently contains a catalytic triad composed of serine, histidine, and aspartic acid residues.[2–5] $LPLA_2$ also has 50% sequence identity with lecithin-cholesterol acyltransferase (LCAT) and shares many structural similarities including distinctive “membrane-binding” and “cap” domains inserted into loops of the hydrolase fold (Figure 1).[6,7] Both enzymes are both *N*-glycosylated with high mannose-type oligosaccharides.[8] Atomic structures of $LPLA_2$ have been solved from multiple crystal forms including fully glycosylated, deglycosylated, and soaked or co-crystallized with fluorophosphonate inhibitors.[3] The co-crystal structure with isopropyl dodecylphosphonofluoridate (IDFP) also revealed two putative lipid acyl-chain binding tracks (referred to as A and B, PDB entry 4X91).[6]

Herein we report a novel crystal structure of $LPLA_2$ with Zn^{2+} directly coordinated by the catalytic serine and histidine in the active site (Figure 1). The binding of the cation occurs concomitantly with closure of the lid loop into the active site in a manner that impedes substrate access. Additionally, we observed that Zn^{2+} inhibits $LPLA_2$ esterase activity at neutral or higher pH. Zn^{2+} has not been previously shown to bind to $LPLA_2$ or affect its activity.[8] The inhibition of $LPLA_2$ by Zn^{2+} could play a regulatory role physiologically because the enzyme is secreted from macrophages before it is reinternalized and targeted to lysosomes where it performs a catabolic role.[9] Whereas $LPLA_2$ shows minimal transacylase activity at neutral and higher pH, it is still able to act as an esterase on soluble substrates such as *p*-nitrophenyl butyrate (pNPB)[10,11] and oxidized phospholipids.[12] Therefore, Zn^{2+} in plasma could act to inhibit the activity of $LPLA_2$ and keep the enzyme from hydrolyzing inappropriate ester substrates before it is reabsorbed by a macrophage. Although $LPLA_2$ would encounter high concentrations of Zn^{2+} in the lysosome, which serves as a Zn^{2+}

storage depot for the cell,[13] the pH dependency of its inhibition by Zn^{2+} would still allow it to perform beneficial catabolic roles in lipid homeostasis.

MATERIALS AND METHODS

Materials.

pNPB was purchased from Sigma-Aldrich (St. Louis, MO) and a 5.6 M stock solution was prepared in chloroform. SYPRO Orange was purchased from ThermoFisher (Waltham, MA). Crystallization screens Classics Lite Suite and JCSG+ Suite were purchased from Qiagen (Venlo, Netherlands) and Index HT from Hampton Research (Aliso Viejo, CA). Gibco Freestyle 293 Expression Medium and Opti-MEM Reduced Serum Media were purchased from ThermoFisher (Walthma, MA). The oxidized lipids, 1-palmitoyl-2-azelaoyl-sn-glycero-3-phosphocholine (PAzePC) and 1-hydroxy-2-azelaoyl-sn-glycero-3-phosphocholine (2-Aze-LPC) were purchased from Avanti Polar Lipids (Alabaster, AL).

Protein expression and purification.

Mouse $LPLA_{2G}$ was purchased from Proteos (Kalamazoo, MI). Human glycosylated $LPLA_2$ ($LPLA_{2G}$) was expressed in HEK293F cells and purified as previously described[6] with a few modifications as follows (UniProt ID: Q8NCC3). HEK293F cells were grown in Freestyle media and transfected at a cell density of 1.4×10^6 using a 1:2 molar ratio of DNA to polyethylenimine diluted in Opti-MEM media. Media was harvested after 5 d, filtered, and loaded onto two 5 mL Ni-NTA columns in batches. The N-terminal His tag was cleaved by the addition of tobacco-etch virus protease to a final concentration of 5% w/w of total protein present in the elution and dialyzed overnight at 4 °C against 20 mM HEPES pH 7.5, 150 mM NaCl, and 1 mM dithiothreitol. Deglycosylated enzyme ($LPLA_{2D}$) was generated by incubation with endoF1 overnight at 4 °C in a 1:10 molar ratio of endoF1:$LPLA_2$. Protein was then further purified by passage over a second Ni-NTA column to remove the His6-tagged endoF1 and concentrated to 8–10 mg/mL.

Protein crystallization.

$LPLA_{2D}$ (8.2 mg/mL) was incubated with 2 mM 2-Aze-LPC on ice for 30 min prior to setting sitting-drop crystallization screens at 4 °C. Crystals were obtained within one week in a condition from the JCSG+ Suite: 100 mM sodium cacodylate pH 6.5, 10% isopropanol, 200 mM zinc acetate. Crystals were reproduced using the hanging drop method with 100 mM sodium cacodylate pH 6.5, 6–10% isopropanol, 200–300 mM zinc acetate and cryoprotected with reservoir solution supplemented with 35% (w/v) sucrose before freezing on nylon loops in liquid N_2.

Structure determination and refinement.

Data was collected at the Argonne Photon Source at Argonne National Laboratories using LS-CAT beam line 21-ID-D (Table 1). Data integration and scaling was performed with DIALS.[14] The structure was solved using Phaser with chain A of PDB ID 4X90 as the search model.[15] Reciprocal-space refinement was performed with the phenix.refine program of PHENIX[16] and alternated with local real-space refinement and model building with Coot.

[17] The final model was validated with MolProbity prior to deposition in the Protein Data Bank under accession code: 6MTW.[18]

Differential scanning fluorimetry (DSF).

$LPLA_{2D}$ (0.2 mg/mL) was mixed with 1X SYPRO dye, 1 mM CHAPS, 5 mM $MgCl_2$, 2 mM DTT, and 20 mM HEPES pH 8.0, in the presence or absence of 200 μM zinc acetate. Samples were heated from 25 to 95 °C with a 2% ramp rate in a 7900HT Fast rtPCR system (Applied Biosystems, Foster City, CA). Plate fluorescence was measured at 475 nm. Melting curves were normalized with 0% as the smallest mean in each data set and 100% as the largest mean in each data set. The T_m was determined by performing a four-parameter variable-slope nonlinear fit of the normalized data in GraphPad Prism. Each experiment was performed on two separate days in triplicate. The T_m is reported as a mean ± SD.

Zn^{2+} IC_{50} Determination.

$LPLA_{2D}$ or $LPLA_{2G}$ was mixed with varying concentrations of zinc acetate or zinc chloride in concentrations ranging from 0 to 500 μM in 20 mM HEPES pH 7.5, 150 mM NaCl at a final protein concentration of 0.1 μM. Reactions were performed in 384-well plates and initiated by mixing 40 μL of the protein mixture with 10 μL of the substrate 10 mM pNPB in 20 mM HEPES pH 7.5, 150 mM NaCl and 10% DMSO. The change in absorbance at 400 nm was monitored for 18 min on a FlexStation 3 Multi-Mode Microplate Reader (Molecular Devices, San Jose, CA), and a linear regression was performed to obtain slopes. These slopes were converted to V_o with units of μM of *p*-nitrophenol (pNP) per min, using a pathlength of 4.1 mm (for a 50 μL reaction in a flat-bottom 384-well plate) and an extinction coefficient of 18 $mM^{-1}cm^{-1}$. V_o was normalized for each individual experiment (where 0% was set as Y=0), plotted against the logarithm of $[Zn^{2+}]$, and the IC_{50} was determined by performing a nonlinear regression using the three-parameter log(inhibitor) vs response equation in GraphPad Prism. Each experiment was performed in triplicate and repeated six times.

Zn^{2+} Michaelis-Menten Kinetic Analysis.

$LPLA_{2D}$ (final concentration of 0.1 μM) was mixed with zinc acetate in concentrations ranging from 0 to 400 μM in 20 mM HEPES pH 7.5, and 150 mM NaCl. Reactions were performed in 384-well plates and initiated by mixing 40 μL of the protein mixture with 10 μL pNPB at varying concentrations (final concentrations from 0.2–8 mM) in 20 mM HEPES pH 7.5, 150 mM NaCl, and 10% DMSO. The reactions were performed at 24 ºC during which absorbance at 400 nm was monitored for 18 min and V_o was calculated as described above. Linear regression of the Lineweaver-Burk plot was performed to determine the inhibition model. The plot of V_o versus [substrate] was subjected to nonlinear regression using a noncompetitive inhibition model in GraphPad Prism to obtain V_{max}, K_i, and K_M. Each experiment was performed in triplicate and repeated three times. Competitive inhibition was ruled out due to the dose-dependent decrease in V_{max} that was observed. Additionally, the data was fit with mixed-model inhibition to determine an α value, which was determined to be 0.94, which is most consistent with a noncompetitive inhibition model (α=1).

Zn^{2+} Inhibition as a Function of Ionic Strength.

Reactions mixtures of 0.1 μM $LPLA_{2D}$ or $LPLA_{2G}$ and 1 mM zinc acetate were prepared with varying concentrations of NaCl (0, 50, 150, and 250 mM) in 20 mM HEPES pH 7.5. Reactions, performed in triplicate, were initiated by mixing 40 μL of the protein mixture with 10 μL of 10 mM pNPB and monitored for 18 min by reading the absorbance at 400 nm.

Zn^{2+} Inhibition as a Function of pH.

Reaction mixtures containing 0.1 μM $LPLA_{2D}$ or $LPLA_{2G}$, 20 mM citrate (pH 4.0, 4.5, and 5.0), MES (pH 5.5, 6.0, and 6.5), or HEPES (pH 7.0, 7.5, and 8.0) buffer were prepared and used as negative controls. Reaction mixes were then supplemented with 150 mM NaCl and/or 1 mM zinc acetate. 10 μL of 10 mM pNPB was added to 40 μL of the reaction mix and reactions were quenched after 18 min with 4% SDS in 0.2 M $NaHCO_3$ and the absorbance read at 400 nm. Reactions were performed in triplicate and repeated three times.

Zn^{2+} Inhibition of Lipase Activity.

$LPLA_2$ hydrolysis of a oxidized lipid substrate (PAzePC) was measured in the presence of zinc acetate using a variation of a previously published method.[12] Reaction mixtures were prepared in 20 mM HEPES pH 7.5, 150 mM NaCl containing 10 μg/mL BSA, 130 μM PAzePC, and varying concentrations of zinc acetate (0–1.5 mM). Reactions were initiated with the addition of $LPLA_{2D}$ or $LPLA_{2G}$ (150 μg/mL final concentration). Reactions were incubated on ice for 30 min, then at 37 °C for 90 min, and terminated by adding 3 mL of 2:1 chloroform:methanol and 0.3 mL of 0.9% (w/v) NaCl. The terminated reaction mixtures were centrifuged at 800 ×*g* for 5 min and the resulting organic layer was transferred to a glass tube and dried down under a stream of nitrogen gas. The dried lipids were resuspended in 40 μL 2:1 chloroform:methanol and applied to HPTLC (high-performance thin-layer chromatography) plates. Plates were developed in a solvent system consisting of chloroform/methanol/pyridine (98:2:0.5, v/v) to visualize the release of palmitic acid and a solvent system consisting of chloroform/methanol/water (60:35:8, v/v) for lysophospholipid products. The plates were dried and soaked in 8% (w/v) $CuSO_4{\cdot}5H_2O$, 6.8% (v/v) H_3PO_4, and 32% (v/v) methanol. The uniformly wet plates were briefly dried with a hair dryer and charred for 15 min in a 150 °C oven. The plates were scanned, and the products were quantified against palmitic acid standards using ImageJ (version 1.37). Values were averaged from at least 4 separate experiments.

RESULTS

Crystal structure of $LPLA_2$ bound to Zn^{2+}.

A novel crystal form of $LPLA_2$ with two proteins in the asymmetric unit was obtained in the presence of the oxidized lipid product 2-Aze-LPC and zinc acetate and diffracted to 2.0 Å spacings (Table 1). Although the presence of 2-Aze-LPC was required for formation of these crystals, no density for the lipid was observed. Thus, we speculate that it plays a detergent-like role in promoting crystallization. Strong positive density (Figure 2A) was observed in the active site was modeled as Zn^{2+} tetrahedrally coordinated to Ser165 and His359 and 2 water molecules (Figure 2B). Three other strong positive density peaks in a crystal contact

were modeled as Zn^{2+} being coordinated by Asp307 and Cys322 of one chain and Glu110 and His106 of the second (Figure 2C, D). The positive omit map electron density peak heights range from 21 to 23 σ for these atoms, consistent with the peaks corresponding to Zn^{2+}.

A large conformational change of the lid loop (residues 210–220) is observed in the $LPLA_2{\cdot}Zn^{2+}$ complex relative to the apo $LPLA_2$ structure (PDB entry 4X90).[6] Comparison of the $LPLA_2{\cdot}Zn^{2+}$ complex to other previously published $LPLA_2$ structures (represented by PDB entries 4X90, 4X93, and 4X97) reveals at least three distinct lid loop conformations (Figure 3A), with the lid loop conformation observed for $LPLA_2{\cdot}Zn^{2+}$ being most similar to a tetragonal ($P4_32_12$) crystal form of $LPLA_2$ in complex with the inhibitor methyl arachidonyl fluorophosphonate (MAFP) (PDB entry 4X93). However, the side chain of Arg214 points toward solvent in the MAFP complex. Contrarily, $LPLA_2$ soaked with MAFP (PDB entry 4X97) displays the most open lid loop conformation, wherein it is shifted outward 7.5 Å from the active site (measured for the Cα of Arg214). The lid loop conformations observed for ligand-free $LPLA_2$ (PDB entry 4X90) thus seems to represent an intermediate state between the most open and closed conformations.

In the LPLA2·Zn^{2+} complex, the lid loop collapses into the active site a maximum of 4.2 Å (Cα of Val217) relative to ligand-free $LPLA_2$. Arg214, which is proposed to make polar interactions with lipid head groups,[11] shifts into the active site by 3.3 Å and forms a hydrogen bond with the backbone of Asp13 (2.6 Å) and thus occludes the beginning of track B (Figure 3B). Asp211 in the lid loop forms a hydrogen bond with Lys202 (2.8 Å), analogous to the interaction between Asp227 and Lys218 in the most closed structure reported for the related enzyme LCAT (PDB entry 5TXF).[19] The inward movement of the lid loop also packs the side chains of three hydrophobic residues (Ile 215, Val217, and Ile218) into a hydrophobic cleft in the membrane-binding domain. We expect Ile215 in this configuration would block acyl chains longer than 12 carbons from binding in track B.

Stabilization of $LPLA_2$ by Zn^{2+}.

Due to the conformational changes observed in the $LPLA_2{\cdot}Zn^{2+}$ complex, we hypothesized that Zn^{2+} can thermally stabilize the enzyme. Indeed, when DSF was performed to determine the melting point (T_m) for $LPLA_2$, we observed a 4° increase in the presence of Zn^{2+} (Figure 4A).

Zn^{2+} inhibition of $LPLA_2$ activity.

We hypothesized that Zn^{2+} binding to catalytic triad residues Ser165 and His359 would inhibit catalytic activity at neutral pH and above due to the pK_a of histidine. We thus monitored the hydrolysis of pNPB, a soluble ester substrate efficiently cleaved by $LPLA_2$, to assay activity in the presence of increasing concentrations of zinc acetate at pH 7.5 (Figure 4B). Zinc chloride exhibited the same inhibition as zinc acetate, confirming that Zn^{2+} was the inhibitory ion. We also tested both the deglycosylated ($LPLA_{2D}$) and glycosylated ($LPLA_{2G}$) forms of $LPLA_2$ to ensure that the Zn^{2+} binding we observed in the crystal complex could occur with the more physiological form of the enzyme. Dose-dependent inhibition of $LPLA_2$ esterase activity by Zn^{2+} was observed with an IC_{50} of 76 ± 20 μM and

53 ± 10 μM for $LPLA_{2D}$ and $LPLA_{2G}$ respectively (Figure 4B), which are not significantly different (p = 0.06) according to a two-tailed unpaired t test. For further kinetic analysis we chose to use $LPLA_{2D}$ as it more stable in solution and has higher activity in the pNPB assay.

Michaelis-Menten kinetics were measured in order to determine the mode of inhibition of 0.1 μM $LPLA_2$ by Zn^{2+}. Seven concentrations of the pNPB substrate were tested with eight concentrations of zinc acetate including a buffer only control. The Lineweaver-Burk plot (Figure 5A) and a nonlinear regression using a mixed-model inhibition were most consistent with a noncompetitive inhibition model ($\alpha = 0.94$). Therefore, the data was fit with noncompetitive inhibition nonlinear regression to determine the kinetic parameters (Figure 5B). A k_{cat} of 2.2 ± 0.05 s^{-1} and a k_{cat}/K_m of 3100 ± 300 $M^{-1}s^{-1}$ were obtained from the 0 μM zinc acetate condition and a K_i of 310 ± 30 μM.

The effect of pH and ionic strength on Zn^{+2} inhibition of $LPLA_2$.

The inhibition of $LPLA_2$ esterase activity by Zn^{2+} was found to be strongly dependent on ionic strength. There was no significant inhibition of $LPLA_{2D}$ or $LPLA_{2G}$ by 1 mM zinc acetate in 20 mM HEPES pH 7.5 buffer lacking NaCl (Figure 6A and B). Zn^{2+} inhibition was imposed by the addition of at least 50 mM NaCl to the buffer. Additionally, background $LPLA_{2D}$ esterase activity was observed to increase in the presence of NaCl, which we presume is due to an improved solvation of the protein at higher ionic strength. The esterase activity of $LPLA_{2G}$, which contains charged sialic acid moieties, was significantly increased only at the highest NaCl concentration tested, 250 mM. The enzyme was completely inhibited by 1 mM zinc acetate in buffer supplemented with 50, 150, or 250 mM NaCl. $LPLA_{2D}$ activity was significantly inhibited by 1 mM zinc acetate at pH 7.0 (63% inhibition), 7.5 (80% inhibition), and 8.0 (85% inhibition) but below pH 7.0 the inhibition dropped sharply (Figure 6C). At pH 6.5, only 30% inhibition is observed, and at pH 6.0 and below there is no significant inhibition of esterase activity. This trend closely follows the pK_a of histidine (approximately 6.0), which transitions from a neutral sidechain to a positively charged imidazole as pH lowers. A similar trend was observed with $LPLA_{2G}$, with significant inhibition by 1 mM zinc acetate observed only at pH 7.0 (47% inhibition), 7.5 (61% inhibition), and 8.0 (73% inhibition) (Figure 6D). When the same pH profiles were tested at 0 mM NaCl no significant inhibition of $LPLA_2$ activity by Zn^{2+} was observed at any pH tested (Figure 6E and F).

Zn^{2+} inhibition of $LPLA_2$ hydrolysis of an oxidized lipid substrate.

At a neutral pH, $LPLA_2$ is unable to efficiently process phospholipids such as DOPC because of its inability to engage anionic membranes, but can efficiently cleave soluble oxidized phospholipids, such as PAzePC.[12] Thus, we assayed the hydrolysis of PAzePC by $LPLA_2$ in the presence of zinc acetate to determine if Zn^{2+} is able to inhibit the processing of a lipid substrate. The release of palmitic acid from the oxidized phospholipid was quantified from HPTLC plates (Figure 7A and B). Significant inhibition of $LPLA_{2D}$ was observed at 0.5, 1.0, 1.2, and 1.5 mM Zn^{2+} (38%, 66%, 86%, 91% inhibition, respectively) (Figure 7C). The same concentrations of Zn^{2+} significantly inhibited $LPLA_{2G}$ by 49%, 47%, 64%, and 86%, respectively.

DISCUSSION

A novel crystal structure of $LPLA_2$ was determined in which there are four Zn^{2+} ions bound to each monomer, one of which is bound in the active site (Figure 1). This latter Zn^{2+} was the focus of the remainder of our study because it directly coordinates two catalytic residues, Ser165 and His359, which are part of the α/β-hydrolase catalytic triad and would therefore be expected to inhibit activity. We also observed a large conformational change of the lid loop (residues 210–220) in this structure relative to the ligand free enzyme. Recently, a structure of the closely related LCAT was determined in which the lid loop forms hydrophobic latch-like interactions that prevent access to the active site (PDB entry 5TXF).[19] The lid loop of the $LPLA_2{\cdot}Zn^{2+}$ complex, although distinct from that of LCAT, would similarly prevent substrate binding. The guanidinium group of Arg214 packs between the side chains of Leu14 and Ile360 in track B and forms a hydrogen bond with the backbone carbonyl of Asp13 (Figure 3), thereby blocking binding of phospholipid and the acyl acceptor *N*-acetylsphingosine for its transacylase reaction.[6] Additionally, the side chains of Ile215, Val217, and Ile218 in the lid loop are shifted downwards into a hydrophobic cleft formed by the side chains of Trp43, Leu44, Leu49, and Trp57. Therefore, this closed conformation would also block longer acyl chains in phospholipid substrates from binding into track B. There is, however, no obvious explanation as to why Zn^{2+} stabilizes this particular state as it makes no direct contacts with the lid loop. The lid loop is also free of crystal contacts that may influence or trap it in this conformation. Regardless, DSF showed the melting temperature of $LPLA_2$ increased 4 °C in the presence of Zn^{2+} (Figure 4A), consistent with the stabilization of a more rigid conformation of the enzyme, such as might be explained by the more closed lid conformation. Thus, we expect Zn^{2+} would bind to the active site at a neutral or higher pH and may play a role in inhibiting inappropriate hydrolysis by the enzyme serum. Because the enzyme ultimately resides in the lysosome, which is a known Zn^{2+} repository, the low pH would eliminate Zn^{2+} binding due to the protonation of the active-site His359.

We thus hypothesized Zn^{2+} would have an inhibitory effect on $LPLA_2$ esterase and transacylase activity and that this would be highly dependent on pH. Our results at neutral pH showed that Zn^{2+} could inhibit pNPB hydrolysis with high μM affinity and that Zn^{2+} inhibition follows a noncompetitive model (K_i of 310 μM). Zn^{2+} inhibition of paraoxonase was also reported to be noncompetitive although the mechanistic basis for this is not known.[20] A profound effect of ionic strength on Zn^{2+} inhibition was observed (Figure 6), with no Zn^{2+} inhibition observed in the absence of NaCl. We do not have an explanation for this phenomenon but note that 0 mM NaCl is not physiological.

The activity pH profile showed that the inhibitory activity of Zn^{2+} was lost below a pH of 6.5 (Figure 6). Thus, we speculate that Zn^{2+} inhibition may in physiological settings act to diminish $LPLA_2$ esterase activity when it is not in an acidic environment such as the lysosome. The lysosome is a Zn^{2+} reservoir which clears toxic levels of Zn^{2+} from the cytoplasm.[13] However, because $LPLA_2$ is not inhibited by up to 1 mM concentrations of Zn^{2+} below a pH of 6.5, the enzyme activity would be less affected by higher concentrations of Zn^{2+} experienced in the lysosome. Serum concentrations of free Zn^{2+} are reported to be around 15 μM,[21] although total Zn^{2+} is higher when considering the fraction bound to

proteins. It is unclear just how much inhibition of $LPLA_2$ occurs in human serum via this mechanism, however we expect that $LPLA_2$ would be only partially inhibited by Zn^{2+} in serum. We attempted to measure the effect of EDTA and *N,N,Ń,Ń*-tetrakis(2-pyridinylmethyl)-1,2-ehtanediamine, a Zn^{2+} specific chelator, on the activity of $LPLA_2$ in human serum but were unable to achieve clear results due to several complicating factors, including high background esterase activity in serum. However, we expect that $LPLA_2$ esterase activity would be at least partially inhibited by Zn^{2+} in serum. To test this idea, we demonstrated that Zn^{2+} can significantly inhibit the hydrolysis of an oxidized phospholipid (PAzePC) by $LPLA_2$ at a neutral pH (Figure 7) starting at 500 μM (40% inhibition).

Other α/β-hydrolases, including paraoxonase, are known to be significantly inhibited by Zn^{2+}, but in most cases the mechanism of inhibition has not been explored.[20,22–26] Zn^{2+} inhibition of a PLA2-like protein in snake venom has previously been investigated using X-ray crystallography and was found to involve coordination to a histidine in the catalytic network (PDB ID: 4WTB).[26] Zn^{2+} has also been shown to inhibit a Ca^{2+}-dependent PLA_2 by direct competition for the Ca^{2+} binding site.[27] In contrast, Zn^{2+} has been shown to bind to group I PLA_2 enzymes and stimulate their activity, but had no effect on group II PLA_2.[28] However, these enzymes have unrelated folds and catalytic mechanisms to $LPLA_2$, and further, to the best of our knowledge, there are no reported structures in which Zn^{2+} is bound to directly to the catalytic residues of an α/β-hydrolase. Therefore, this structure could represent a novel mechanism for the Zn^{2+} inhibition of $LPLA_2$ and perhaps other enzymes in the same fold class.

Supplementary Material

Refer to Web version on PubMed Central for supplementary material.

Acknowledgments

Funding Sources

This work was supported by US National Institutes of Health (NIH) grants HL071818 and HL122416 (to JJGT). RB is supported by an American Heart Association fellowship (18POST33960047).

ABBREVIATIONS

2-Aze-LPC	1-hydroxy-2-azelaoyl-sn-glycero-3-phosphocholine
CHAPS	3-[(3-cholamidopropyl)dimethylammonio]-1-propanesulfonate hydrate
DSF	differential scanning fluorimetry
EDTA	ethylenediaminetetraacetic acid
endoF1	endoglycosidase F1
HEPES	(4-(2-hydroxyethyl)-1-piperazineethanesulfonic acid
HPTLC	high-performance thin-layer chromatography

IDFP	isopropyl dodecylfluorophosphonte
LCAT	lecithin-cholesterol acyltransferase
LPLA2	lysosomal phospholipase A2
MAFP	methyl arachidonyl fluorophosphonate
MES	2-ethanesulfonic acid
PAzePC	1-palmitoyl-2-azelaoyl-sn-glycero-3-phosphocholine
pNPB	*p*-nitropheyl butyrate

REFERENCES

(1). Hiraoka M, Abe A, Lu Y, Yang K, Han X, Gross RW, and Shayman JA (2006) Lysosomal phospholipase A2 and phospholipidosis. Mol. Cell. Biol 26, 6139–6148. [PubMed: 16880524]

(2). Hiraoka M, Abe A, and Shayman JA (2005) Structure and function of lysosomal phospholipase A2: identification of the catalytic triad and the role of cysteine residues. J. Lipid Res 46, 2441–2447. [PubMed: 16106046]

(3). Vasquez AM, Mouchlis VD, and Dennis EA (2018) Review of four major distinct types of human phospholipase A 2. Adv. Biol. Regul 67, 212–218. [PubMed: 29248300]

(4). Dennis EA, Cao J, Hsu Y-H, Magrioti V, and Kokotos G (2011) Phospholipase A2 Enzymes: Physical Structure, Biological Function, Disease Implication, Chemical Inhibition, and Therapeutic Intervention. Chem. Rev 111, 6130–6185. [PubMed: 21910409]

(5). Shayman JA, and Tesmer JJG (2018) Lysosomal phospholipase A2. Biochim. Biophys. Acta BBA - Mol. Cell Biol. Lipids

(6). Glukhova A, Hinkovska-Galcheva V, Kelly R, Abe A, Shayman JA, and Tesmer JJG (2015) Structure and function of lysosomal phospholipase A2 and lecithin:cholesterol acyltransferase. Nat. Commun 6, 6250. [PubMed: 25727495]

(7). Piper DE, Romanow WG, Gunawardane RN, Fordstrom P, Masterman S, Pan O, Thibault ST, Zhang R, Meininger D, Schwarz M, Wang Z, King C, Zhou M, and Walker NPC (2015) The high-resolution crystal structure of human LCAT. J. Lipid Res 56, 1711–1719. [PubMed: 26195816]

(8). Abe A, and Shayman JA (1998) Purification and Characterization of 1-O-Acylceramide Synthase, a Novel Phospholipase A2 with Transacylase Activity. J. Biol. Chem 273, 8467–8474. [PubMed: 9525960]

(9). Abe A, Kelly R, and Shayman JA (2010) The measurement of lysosomal phospholipase A2 activity in plasma. J. Lipid Res 51, 2464–2470. [PubMed: 20410020]

(10). Hiraoka M, Abe A, and Shayman JA (2002) Cloning and characterization of a lysosomal phospholipase A2, 1-O-acylceramide synthase. J. Biol. Chem 277, 10090–10099. [PubMed: 11790796]

(11). Hinkovska-Galcheva V, Kelly RJ, Manthei KA, Bouley R, Yuan W, Schwendeman A, Tesmer JJG, and Shayman JA (2018) Determinants of pH profile and acyl chain selectivity in lysosomal phospholipase A2. J. Lipid Res 59, 1205–1218. [PubMed: 29724779]

(12). Abe A, Hiraoka M, Ohguro H, Tesmer JJ, and Shayman JA (2017) Preferential hydrolysis of truncated oxidized glycerophospholipids by lysosomal phospholipase A2. J. Lipid Res 58, 339–349. [PubMed: 27993948]

(13). Kukic I, Kelleher SL, and Kiselyov K (2014) Zn2+ efflux through lysosomal exocytosis prevents Zn2+-induced toxicity. J Cell Sci 127, 3094–3103. [PubMed: 24829149]

(14). Gildea RJ, Waterman DG, Parkhurst JM, Axford D, Sutton G, Stuart DI, Sauter NK, Evans G, and Winter G (2014) New methods for indexing multi-lattice diffraction data. Acta Crystallogr. D Biol. Crystallogr 70, 2652–2666. [PubMed: 25286849]

(15). McCoy AJ, Grosse-Kunstleve RW, Adams PD, Winn MD, Storoni LC, and Read RJ (2007) Phaser crystallographic software. J. Appl. Crystallogr 40, 658–674. [PubMed: 19461840]

(16). Adams PD, Afonine PV, Bunkóczi G, Chen VB, Davis IW, Echols N, Headd JJ, Hung L-W, Kapral GJ, Grosse-Kunstleve RW, McCoy AJ, Moriarty NW, Oeffner R, Read RJ, Richardson DC, Richardson JS, Terwilliger TC, and Zwart PH (2010) PHENIX: a comprehensive Python-based system for macromolecular structure solution. Acta Crystallogr. D Biol. Crystallogr 66, 213–21. [PubMed: 20124702]

(17). Emsley P, and Cowtan K (2004) Coot: model-building tools for molecular graphics. Acta Crystallogr. D Biol. Crystallogr 60, 2126–2132. [PubMed: 15572765]

(18). Chen VB, Arendall WB, Headd JJ, Keedy DA, Immormino RM, Kapral GJ, Murray LW, Richardson JS, and Richardson DC (2010) MolProbity: all-atom structure validation for macromolecular crystallography. Acta Crystallogr. D Biol. Crystallogr 66, 12–21. [PubMed: 20057044]

(19). Manthei KA, Ahn J, Glukhova A, Yuan W, Larkin C, Manett TD, Chang L, Shayman JA, Axley MJ, Schwendeman A, and Tesmer JJG (2017) A retractable lid in lecithin:cholesterol acyltransferase provides a structural mechanism for activation by apolipoprotein A-I. J. Biol. Chem 292, 20313–20327. [PubMed: 29030428]

(20). Gonzalvo MC, Gil F, Hernández AF, Villanueva E, and Pla A (1997) Inhibition of paraoxonase activity in human liver microsomes by exposure to EDTA, metals and mercurials. Chem. Biol. Interact 105, 169–179. [PubMed: 9291995]

(21). Savarino L, Granchi D, Ciapetti G, Cenni E, Ravaglia G, Forti P, Maioli F, and Mattioli R (2001) Serum concentrations of zinc and selenium in elderly people: results in healthy nonagenarians/centenarians. Exp. Gerontol 36, 327–339. [PubMed: 11226746]

(22). Novototskaya-Vlasova K, Petrovskaya L, Yakimov S, and Gilichinsky D (2012) Cloning, purification, and characterization of a cold-adapted esterase produced by Psychrobacter cryohalolentis K5T from Siberian cryopeg. FEMS Microbiol. Ecol 82, 367–375. [PubMed: 22486752]

(23). Mohamed YM, Ghazy MA, Sayed A, Ouf A, El-Dorry H, and Siam R (2013) Isolation and characterization of a heavy metal-resistant, thermophilic esterase from a Red Sea Brine Pool. Sci. Rep 3, 3358. [PubMed: 24285146]

(24). Wetterholm A, Macchia L, and Haeggstrom JZ (1994) Zinc and Other Divalent-Cations Inhibit Purified Leukotriene A4 Hydrolase and Leukotriene B-4 Biosynthesis in Human Polymorphonuclear Leukocytes. Arch. Biochem. Biophys 311, 263–271. [PubMed: 8203889]

(25). Wells MA (1973) Spectral perturbations of Crotalus adamanteus phospholipase A $_2$ induced by divalent cation binding. Biochemistry 12, 1080–1085. [PubMed: 4734660]

(26). Borges RJ, Cardoso FF, Fernandes CAH, Dreyer TR, de Moraes DS, Floriano RS, Rodrigues-Simioni L, and Fontes MRM (2017) Functional and structural studies of a Phospholipase A 2 -like protein complexed to zinc ions: Insights on its myotoxicity and inhibition mechanism. Biochim. Biophys. Acta BBA - Gen. Subj 1861, 3199–3209.

(27). Yu B-Z, Rogers J, Nicol GR, Theopold KH, Seshadri K, Vishweshwara S, and Jain MK (1998) Catalytic Significance of the Specificity of Divalent Cations as K_S * and k_{cat} * Cofactors for Secreted Phospholipase A $_2$ †. Biochemistry 37, 12576–12587. [PubMed: 9730830]

(28). Lindahl M, and Tagesson C (1996) Zinc (Zn2+) binds to and stimulates the activity of group i but not group II phospholipase A2. Inflammation 20, 599–611. [PubMed: 8979149]

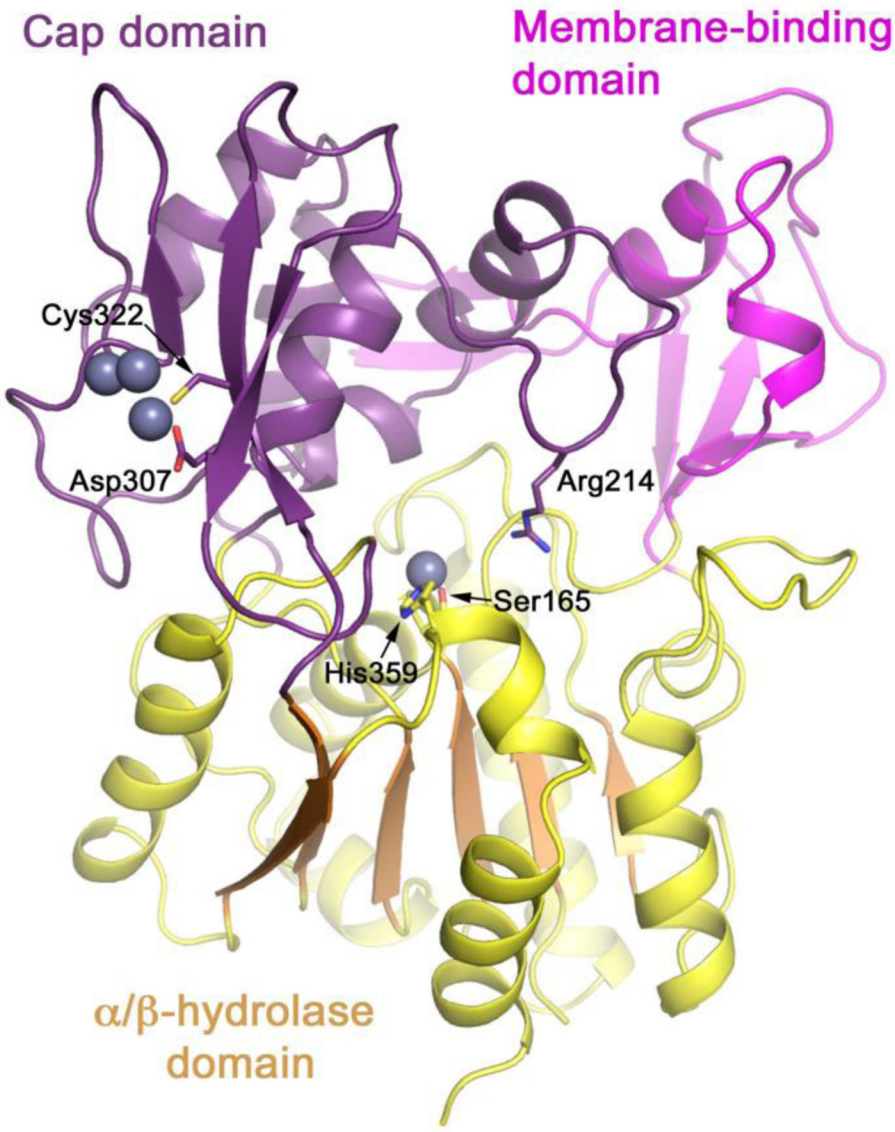

Figure 1.

Zn^{2+} binds in the active site of $LPLA_2$. The α/β hydrolase domain of $LPLA_2$ is shown in yellow with orange β-strands, the membrane-binding domain in magenta, and the cap domain in purple. Zn^{2+} ions are shown as gray spheres. The side chains of residues that interact with the various Zn^{2+} ions (Ser165, His359, Asp307, and Cys322) are shown as stick models. The side chain of Arg214, located in the lid loop is also shown.

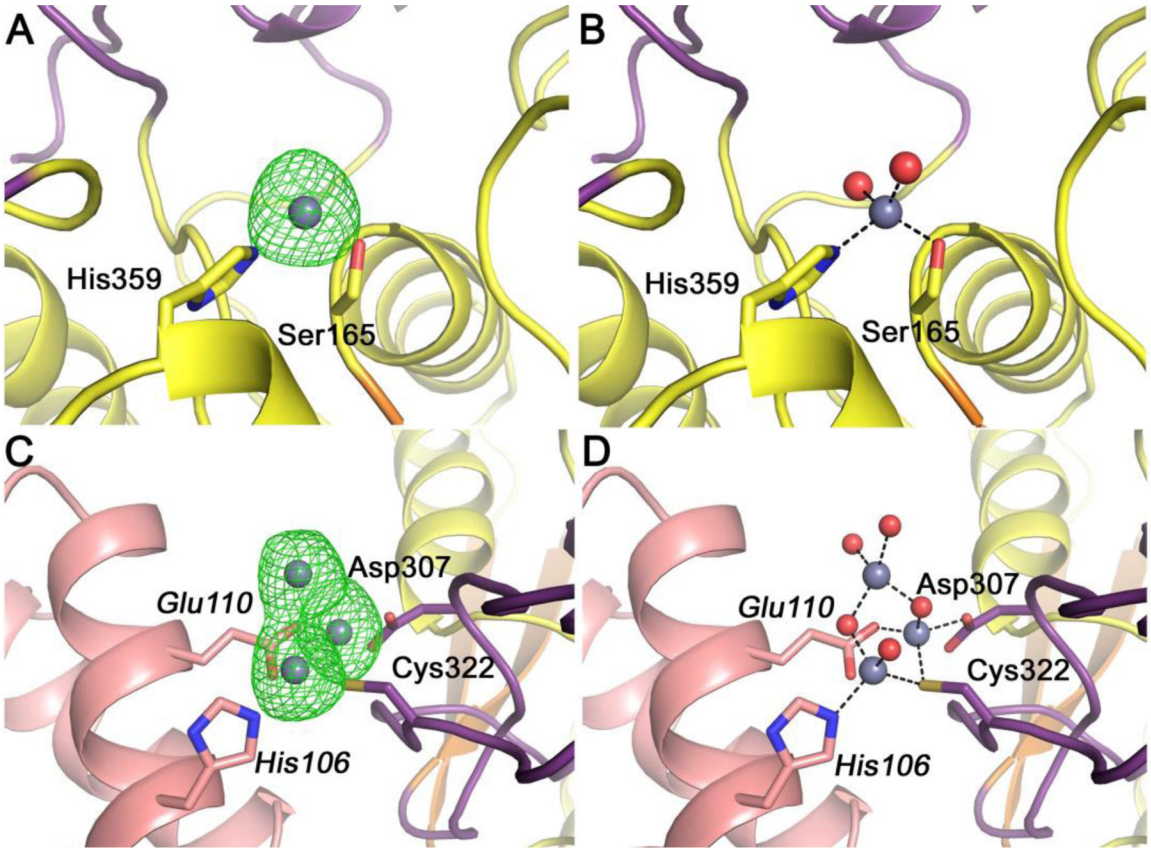

Figure 2.

Zn^{2+} coordination in $LPLA_2$. $|F_o|$-$|F_c|$ omit map shown as a green mesh contoured at 3.0 σ for Zn^{2+} bound in the active site (A), where it is coordinated (back dashed lines) by active site residues, Ser165 and His359, and two water molecules (B). $|F_o|$-$|F_c|$ omit map shown as a green mesh contoured at 3.0 σ for Zn^{2+} cations bound in a crystal contact (C) where three Zn^{2+} cations are coordinated by five water molecules, Asp307 and Cys322 in one protein molecule, and Glu110 and His106 in a symmetry molecule (D). Zn^{2+} ions and waters are shown as gray and red spheres, respectively. The α/β hydrolase domain of the symmetry related protein chain is colored salmon in panels C and D.

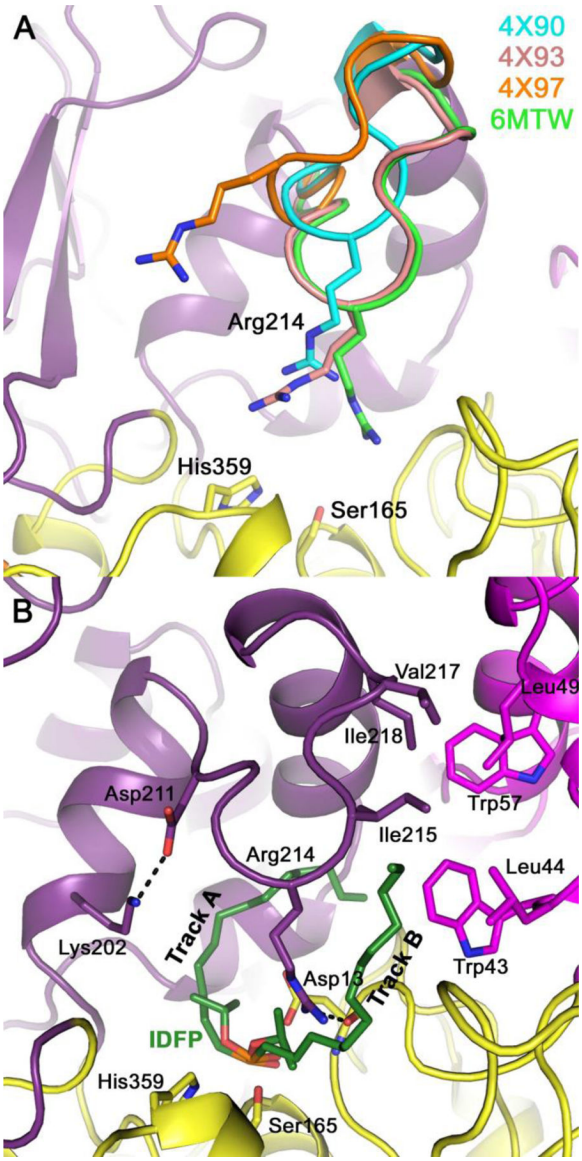

Figure 3.

The lid loop adopts a closed conformation in the LPLA2·Zn^{2+} complex that would interfere with lipid binding. (A) Inward orientation of Arg214 relative to other LPLA2 structures. Lid loop of ligand-free $LPLA_2$ (PDB entry 4X90) is shown in cyan, $P4_32_12$ $LPLA_2$·MAFP (4X93) in salmon, $P1$ $LPLA_2$·MAFP (4X97) in orange, and $LPLA_2$·Zn^{2+} (6MTW) in green. (B) Blockade of track B in the $LPLA_2$·Zn^{2+} complex. IDFP is modeled from the 4X91 structure and depicted as a stick model with green carbons to show the expected path of two acyl tracks (A and B). Hydrogen-bond interactions are shown as black dashed lines. Domains are colored as shown in Figure 1.

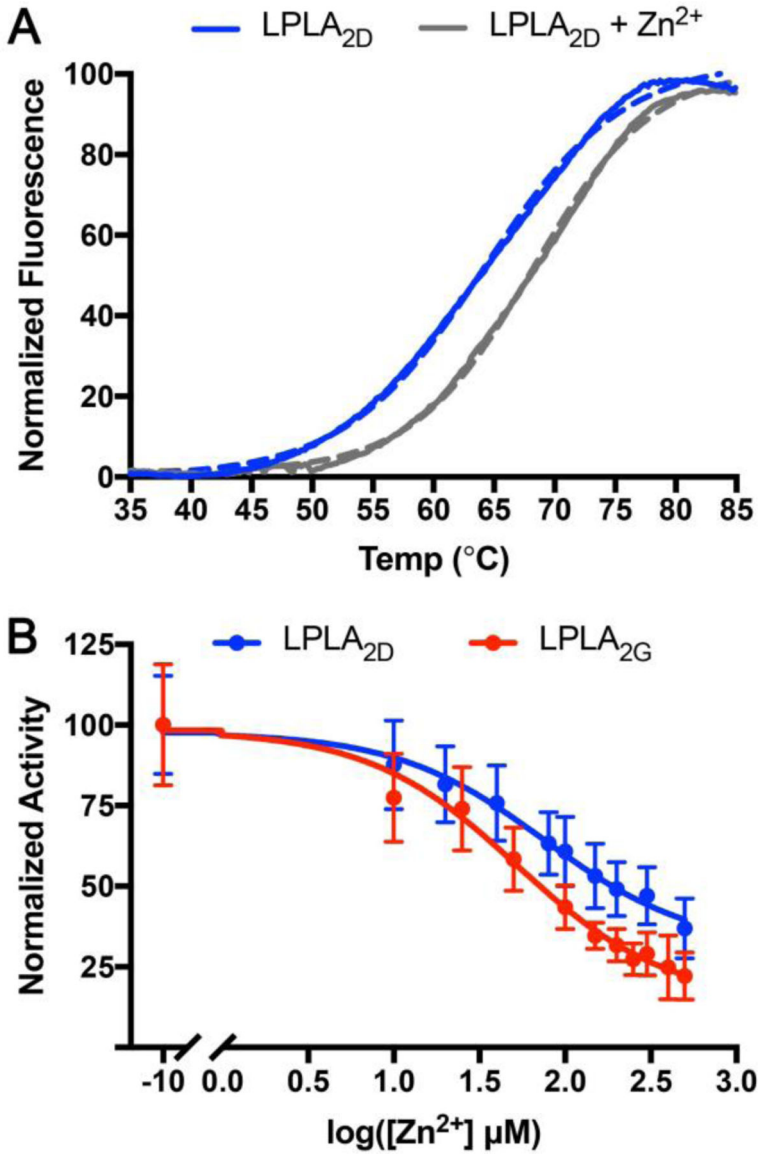

Figure 4.

Zn^{2+} stabilizes $LPLA_2$ and inhibits pNPB hydrolysis at pH 7.5. (A) DSF data from 2 experiments performed in triplicate are shown as solid lines and the nonlinear regression as dashed lines. T_m increased from 64.2 ± 0.4 ºC to 68.2 ± 0.5 ºC in the presence of 200 µM Zn^{2+} (B) Normalized activity (V_o) versus log[Zn^{2+}]. 100% activity corresponds to a V_o of 5.3 ± 1.1 and 2.4 ± 0.6 µM pNP/min for $LPLA_{2D}$ and $LPLA_{2G}$, respectively. For the normalization, 0% activity was set to a V_o of 0 µM pNP/min. Three-parameter nonlinear regressions are shown as solid lines. Data points are averages ± SD from 6 experiments performed in triplicate.

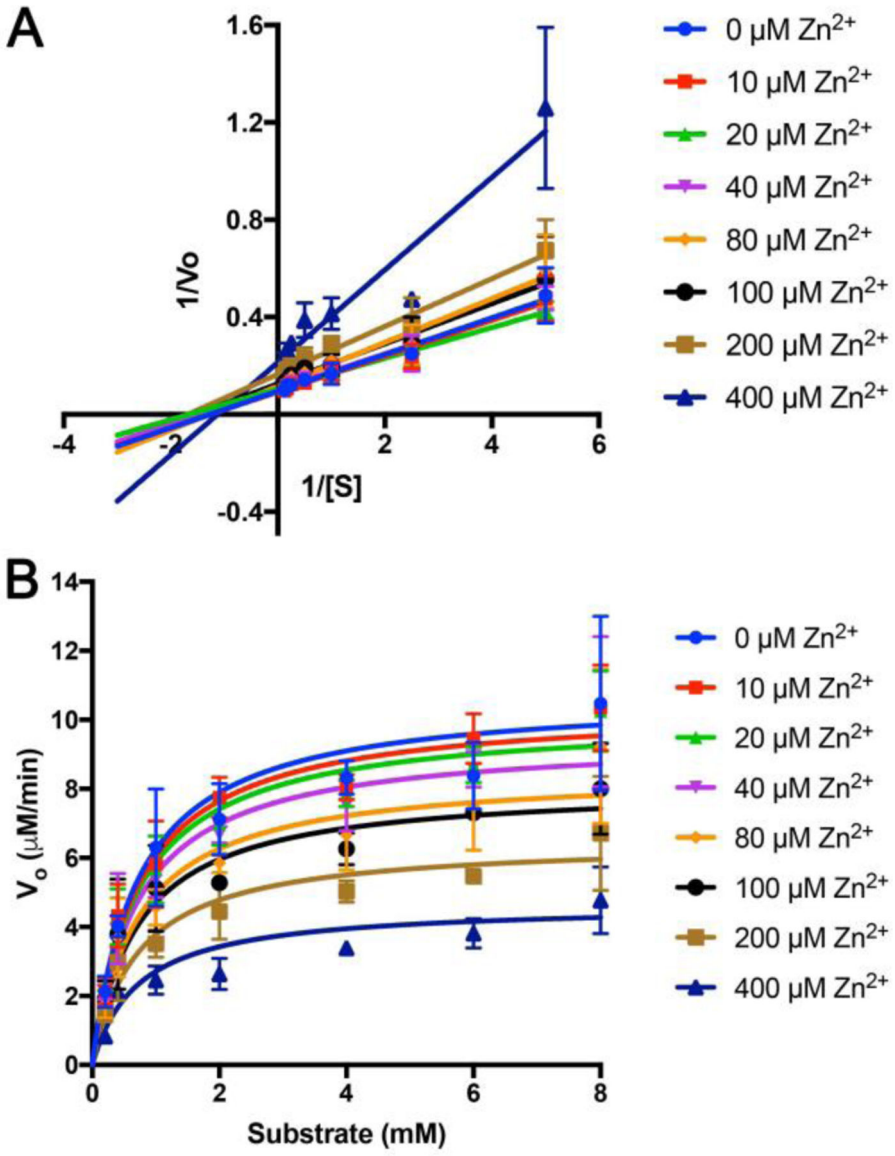

Figure 5.

Kinetic analysis of Zn^{2+} inhibition of $LPLA_{2D}$ reveals noncompetitive behavior. (A) Lineweaver-Burk plot with the linear regression shown as solid lines. (B) Initial velocity versus substrate concentration along with nonlinear regression for a noncompetitive model shown as solid lines. Data points are averages ± SD from 3 experiments performed in triplicate.

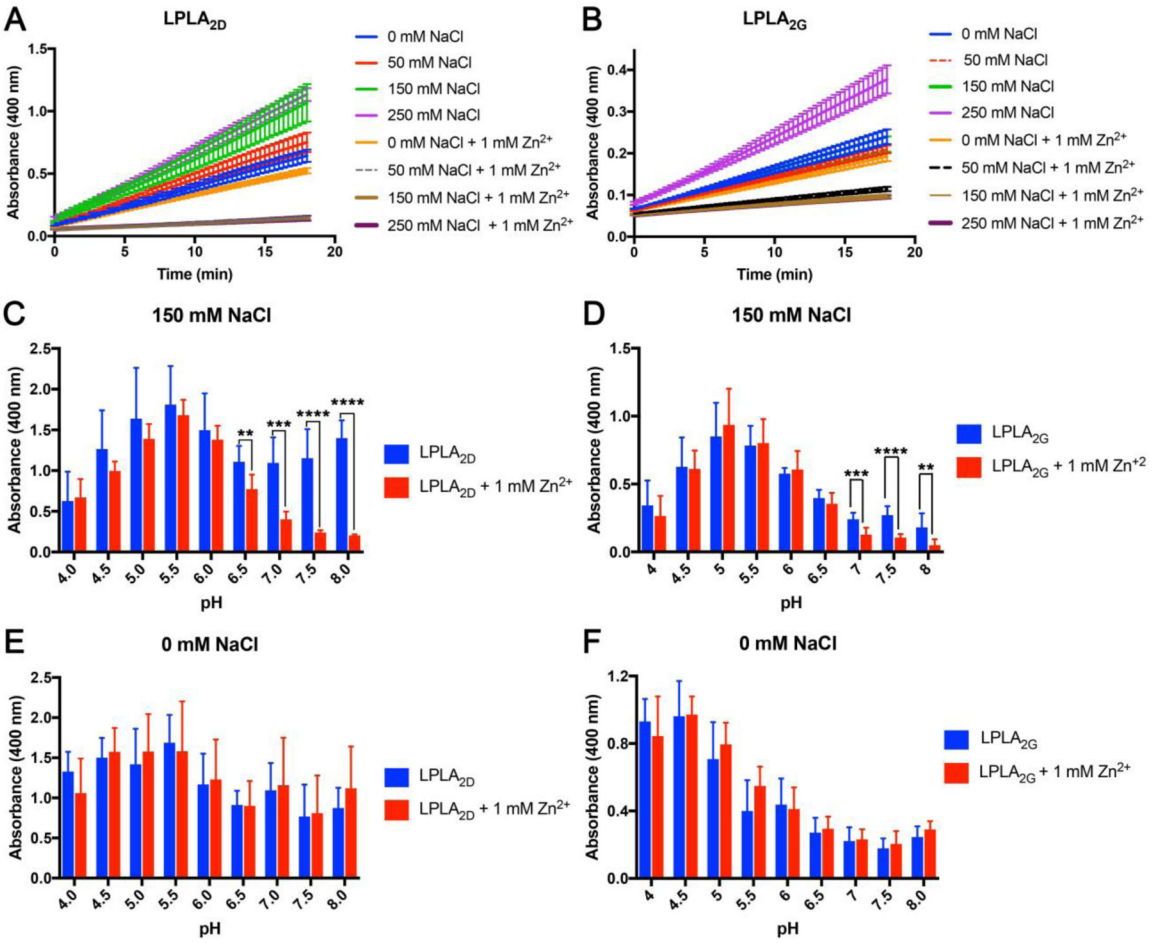

Figure 6.

Higher ionic strength is required for pH-dependent Zn^{2+} inhibition of $LPLA_2$. (A) $LPLA_{2D}$ hydrolysis of pNPB vs. time at various NaCl concentrations ± 1 mM zinc acetate. Data points showing 1 mM Zn^{2+} with 50, 150, and 250 mM NaCl are overlapping. (B) $LPLA_{2G}$ hydrolysis of pNPB vs. time at various NaCl concentrations ± 1 mM zinc acetate. Data points showing 50 mM NaCl and 150 mM NaCl are overlapping. Data points showing 1 mM Zn^{2+} with 150 and 250 mM NaCl are overlapping. (C) Absorbance from pNPB hydrolysis after 18 min at various pH values at 150 mM NaCl ± 1 mM zinc acetate with $LPLA_{2D}$ or (D) $LPLA_{2G}$. (E) Absorbance from pNPB hydrolysis after 18 min at various pH values at 0 mM NaCl ± 1 mM zinc acetate with $LPLA_{2D}$ or (F) $LPLA_{2G}$. In panels C through F, a two-tailed unpaired t test was performed; * $p \leq 0.05$, ** $p \leq 0.01$, *** $p \leq 0.001$, **** $p \leq 0.0001$.

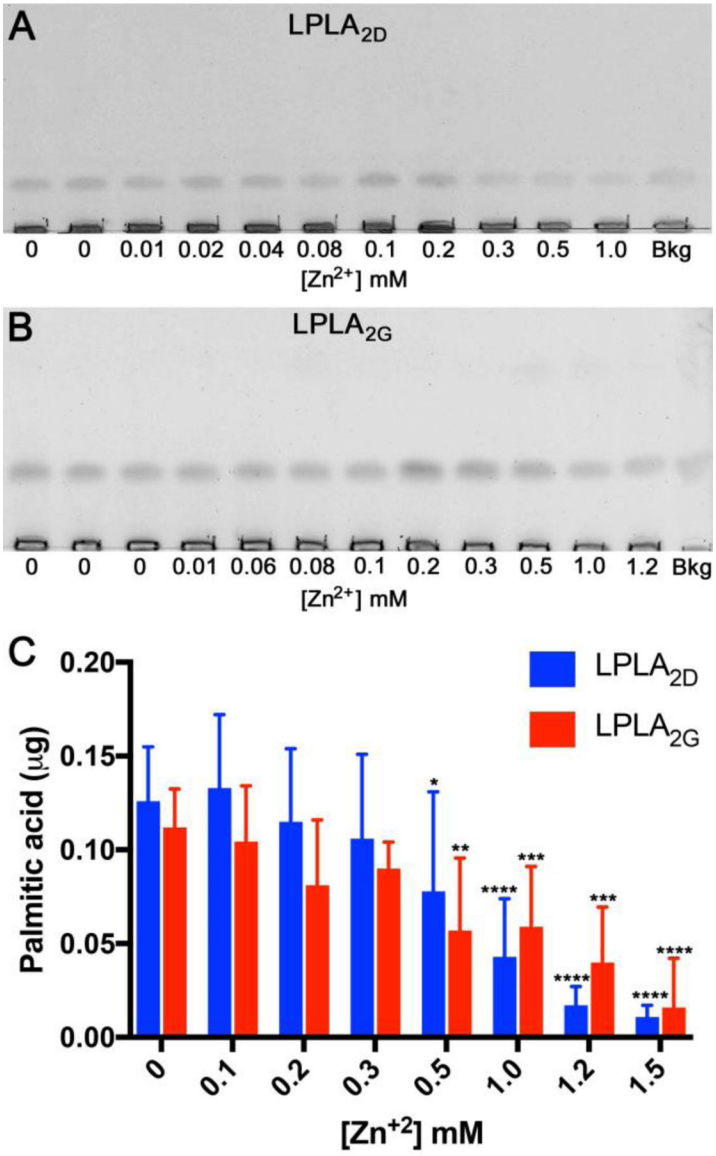

Figure 7.

Zn^{2+} inhibits the hydrolysis of lipidic substrates by $LPLA_2$. The release of palmitic acid from the oxidized phospholipid, PAzePC, was visualized and quantified from HPTLC plates for (A) $LPLA_{2D}$ and (B) $LPLA_{2G}$. The background (Bkg) level of palmitic acid produced in absence of enzyme was subtracted from the band intensities to determine the final values. (C) Summary of palmitic acid data. Values are an average ± SD from at least 4 separate experiments. A two-tailed unpaired t test was performed for each Zn^{2+} condition in comparison with the 0 mM Zn^{2+} control to determine statistical significance; * $p \leq 0.05$, ** $p \leq 0.01$, *** $p \leq 0.001$, **** $p \leq 0.0001$.

Table 1.

Crystallographic data and refinement statistics

X-ray source	APS 21-ID-D
Wavelength (Å)	1.0332
D_{min} (Å)	39.3 – 1.99 (2.07 – 1.99)*
Space group	*R*3
Cell constants (Å)	84.6, 84.6, 322
Unique reflections	57874 (5721)
Multiplicity	5.2 (4.2)
R_{merge} (%)	0.149 (0.525)
Completeness (%)	99.6 (98.1)
$\langle I \rangle / \langle \sigma_I \rangle$	6.94 (2.46)
Total reflections used	57821 (5718)
Protein atoms	6038
Ligand atoms	66
Water molecules	342
RMSD bonds (Å)	0.005
RMSD angles (°)	1.08
Ramachandran favored, outliers (%)	97.3, 0.6
Average *B*-factor (Å^2)	34.7
Protein	34.5
Ligand	39.6
Solvent	36.2
R_{work}	0.248 (0.321)
R_{free}	0.285 (0.333)

*Values for highest resolution shell in parenthesis